Evidence for Band Renormalizations in Strong-Coupling Superconducting Alkali-Fulleride Films

J. S. Zhou,[1,2] R. Z. Xu,[1,2] X. Q. Yu,[1,2] F. J. Cheng,[1,2] W. X. Zhao,[1,2] X. Du,[1,2] S. Z. Wang,[1,2] Q. Q. Zhang,[1,2] X. Gu,[1,2] S. M. He,[3] Y. D. Li,[1,2] M. Q. Ren,[1,2] X. C. Ma,[1,2,6] Q. K. Xue,[1,2] Y. L. Chen,[3,4,5,*] C. L. Song,[1,2,6] and L. X. Yang[1,2,6,†]

[1]*State Key Laboratory of Low Dimensional Quantum Physics, Department of Physics, Tsinghua University, Beijing 100084, China*

[2]*Frontier Science Center for Quantum Information, Beijing 100084, China*

[3]*Department of Physics, Clarendon Laboratory, University of Oxford, Parks Road, Oxford OX1 3PU, United Kingdom*

[4]*School of Physical Science and Technology, ShanghaiTech University and CAS-Shanghai Science Research Center, Shanghai 201210, China*

[5]*ShanghaiTech Laboratory for Topological Physics, Shanghai 200031, China*

[6]*Collaborative Innovation Center of Quantum Matter, Beijing 100084, China*

(Received 5 October 2022; revised 6 February 2023; accepted 17 April 2023; published 26 May 2023)

There has been a long-standing debate about the mechanism of the unusual superconductivity in alkali-intercalated fullerides. In this Letter, using high-resolution angle-resolved photoemission spectroscopy, we systematically investigate the electronic structures of superconducting K_3C_{60} thin films. We observe a dispersive energy band crossing the Fermi level with the occupied bandwidth of about 130 meV. The measured band structure shows prominent quasiparticle kinks and a replica band involving the Jahn-Teller active phonon modes, which reflects strong electron-phonon coupling in the system. The electron-phonon coupling constant is estimated to be about 1.2, which dominates the quasiparticle mass renormalization. Moreover, we observe an isotropic nodeless superconducting gap beyond the mean-field estimation ($2\Delta/k_BT_c \approx 5$). Both the large electron-phonon coupling constant and large reduced superconducting gap suggest a strong-coupling superconductivity in K_3C_{60}, while the electronic correlation effect is suggested by the observation of a waterfall-like band dispersion and the small bandwidth compared with the effective Coulomb interaction. Our results not only directly visualize the crucial band structure but also provide important insights into the mechanism of the unusual superconductivity of fulleride compounds.

DOI: 10.1103/PhysRevLett.130.216004

Alkali-intercalated fullerides A_3C_{60} (A = K, Rb, Cs) not only record the superconducting transition temperature among the molecular superconductors [1–7] but also exhibit many unusual properties that resemble cuprate and iron-based high-temperature superconductors, such as domed superconducting phase diagram [4], the proximation to a magnetic Mott-insulating parent state [8–13], and the formation of a pseudogap [14]. After extensive research efforts, the mechanism of the superconductivity in fullerides, however, remains controversial due to the strong entanglement of the electronic correlation effect and complicated electron-phonon coupling (EPC). While fulleride superconductors were arguably considered to be conventional Bardeen-Cooper-Schrieffer (BCS) superconductors [15–18], many unconventional superconducting mechanisms have been proposed [11–13,19–21], including polaron-driven superconductivity [22,23], local pairing with Jahn-Teller phonons assisted by Coulomb repulsion [13,24], negative Hund's coupling stabilized by EPC [25], and pure electronic pairing [26]. The interplay between microscopic interactions underlying the electronic phase diagram of fullerides also remains elusive to date.

To understand the unusual superconductivity in fullerides, it is highly desired to investigate their electronic structure in the energy-momentum space. From the electronic structure perspective, the lowest unoccupied molecular orbital (LUMO) of the C_{60} molecule is of t_{1u} symmetry [17]. Jahn-Teller distortion with possible D_{2h} symmetry further lifts the degeneracy of the t_{1u} bands and the three electrons donated by alkali atoms populate the split b_{2u} and b_{3u} bands of A_3C_{60}, inducing a low-spin $S = ½$ ground state [11]. The conduction bandwidth W is shown to be much smaller than the effective Coulomb interaction U [27,28], and a Mott-Jahn-Teller insulator phase is discovered in Cs_3C_{60} [8–12]. These observations suggest an important role of the electronic correlation in the electronic properties of A_3C_{60} [11–13], although no Mott localization is observed in superconducting K_3C_{60} and Rb_3C_{60}. Despite these important experimental and theoretical breakthroughs, direct measurement of the electronic

band structure and its coupling to phonon modes is still essentially lacking due to the lack of high-quality crystal surfaces. The momentum distribution of the superconducting gap is also yet to be experimentally investigated.

In this Letter, we overcome the obstacle of the sample-surface quality by synthesizing high-quality thin films of K-intercalated C_{60} on bilayer graphene and systematically investigate their electronic structures using high-resolution angle-resolved photoemission spectroscopy (ARPES). We present the evolution of the electronic structure with film thickness, K-doping, and temperature. While the electronic structure of slightly K-doped C_{60} shows a large insulating gap, K_3C_{60} exhibits a dispersive band crossing the Fermi level (E_F), which is strongly renormalized by multiple phonon modes, directly evidencing the strong EPC in the system. Interestingly, we observe a replica band due to the formation of polarons involving the Jahn-Teller active $H_g(8)$ phonon at about 192 meV. In the superconducting state, we observe an isotropic nodeless superconducting gap, suggesting an *s*-wave superconducting pairing. The magnitude of the reduced superconducting gap $2\Delta/k_BT_c \approx 5$ is beyond mean-field estimation, which, together with a large EPC constant of 1.2, suggests a strong-coupling superconductivity in K_3C_{60}. In addition, we observe waterfall-like band dispersion in a large energy scale, alluding the importance of electronic correlation in the system, which is supported by the small ratio between the bandwidth W and effective Coulomb interaction U. Our results not only directly visualize the long-sought crucial electronic structure of superconducting fullerides but also evidence the strong EPC involving multiple crucial phonon modes, which shed new light on the understanding of the unusual superconductivity of fullerides.

High-quality K_3C_{60} films were prepared on bilayer graphene that was epitaxially grown on silicon carbide using molecular beam epitaxy (MBE) [Fig. 1(a)] [14]. C_{60} films were first synthesized layer-by-layer as monitored by the intensity oscillation of specular spot in the reflection high-energy electron diffraction (RHEED) pattern [Fig. 1(b)]. The K atoms were subsequently deposited on the C_{60} films, followed by a slight annealing at room temperature for an hour so that K atoms can uniformly intercalate the C_{60} films. The films were then *in situ* transferred to ARPES chamber under ultrahigh vacuum below 1.5×10^{-10} mbar. High-resolution ARPES measurements were conducted using a DA30 analyzer and Scienta VUV5050 helium lamp. The energy and angular resolutions were set to 7 meV and 0.2°, respectively.

As schematically shown in Fig. 1(a), K_3C_{60} films crystallize along the [111] direction of a face-centered-cubic (fcc) structure. K atoms occupy either the tetrahedral (green spheres) or octahedral (red spheres) interstitial holes between the hexagonal C_{60} layers. Figure 1(c) shows the surface topography of a 5 monolayer (ML) K_3C_{60} film measured by scanning tunneling microscopy (STM). C_{60}

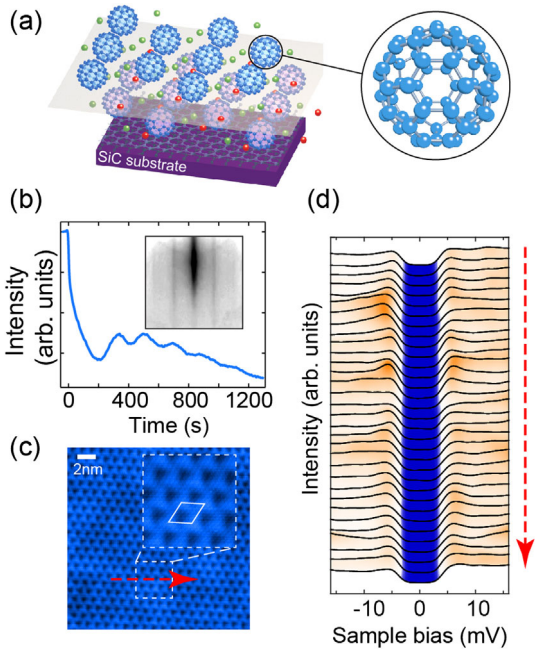

FIG. 1. (a) Schematic illustration of the crystal structure of bilayer K_3C_{60} grown on an epitaxial bilayer graphene that was prepared by graphitizing the SiC substrate. The red and green spheres are the K atoms occupying octahedral and tetrahedral interstitial sites between C_{60} molecules. The zoom-in plot shows a C_{60} molecule with a diameter of about 10 Å. (b) The intensity of the specular spot in RHEED pattern as a function of sample growth time. The film thickness can be monitored by the oscillation in the RHEED curve. (c) STM surface topography of 5 monolayer (ML) K_3C_{60} showing trilobe feature, acquired at sample bias $U = 1.5$ V and a constant tunneling current of $I = 30$ pA. (d) Line profile along the red dashed arrow in (c) showing the homogenous superconducting gap. Data were collected at 4.7 K.

molecules show a uniform configuration with a hexagon facing up as manifested by the tri-lobe-like pattern. We observe no noticeable reconstruction and orientational disorder. The intermolecular distance is about 10.0 ± 0.1 Å, in good agreement with the previous results and the value in bulk fcc K_3C_{60} [14,17,28]. Figure 1(d) shows the scanning tunneling spectroscopy (STS) measured along the dashed line in Fig. 1(c) at 4.7 K, in which the homogenous superconducting gap is clearly observed.

Figure 2 shows the evolution of the band structure of 3 ML C_{60} film along $\bar{\Gamma}\bar{M}$ with K doping. Without C_{60}, the epitaxial bilayer graphene substrate shows a gapped band structure around the $\bar{\Gamma}$ point with the band top at about 2.7 eV below E_F (Supplemental Material, Fig. S1 [29]) [33]. The deposition of C_{60} masks the band dispersion of the substrate and contributes dispersive bands around −2.5 and −3.9 eV, which are derived from the highest occupied molecular orbital (HOMO) and second HOMO (HOMO-1) of C_{60} (Supplemental Material, Fig. S1 [29]) [30,31].

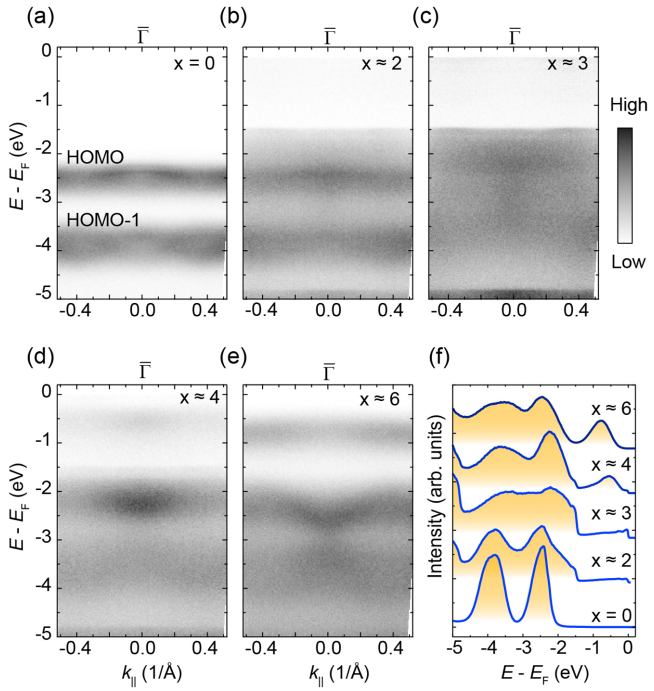

FIG. 2. (a) Band structure of 3 ML pristine C_{60} film grown on bilayer graphene/SiC substrate. (b)–(e) Evolution of the band structure of K_xC_{60} film with K doping. (f) Integrated energy distribution curves (EDCs) of K_xC_{60} films in (a)–(e). Data were collected using a helium lamp ($h\nu = 21.2$ eV) at 13 K.

With K intercalation, the HOMO and HOMO-1 bands shift towards E_F and become more dispersive while the band gap between them shrinks [Figs. 2(b)–2(e)], which alludes an enhanced inter-molecular interaction that may be bridged by alkali metals. Prominently, extra electronic states emerge near E_F in K_3C_{60} due to the population of the LUMO band of C_{60}. These states dominate the density of states (DOS) of K_3C_{60} near E_F and are thus crucial for the superconductivity. The states near E_F in K_2C_{60}, however, are due to the phase separation at slight K doping level (Supplemental Material, Fig. S7 [29]). With further increasing K doping, the spectral weight of the newly emerged states is enhanced but shifts away from E_F [Figs. 2(d)–2(e)], suggesting a metal-to-insulator transition at doping levels much higher than $x = 3$ [28].

To understand the superconducting properties of K_3C_{60}, we investigate the temperature evolution of the fine band structure near E_F in Figs. 3(a)–3(e). We reveal highly dispersive hole band crossing E_F at Fermi momentum $k_F = \pm 0.20 \pm 0.01$ Å^{-1}. This band contributes to the DOS peak near E_F [Fig. 2(f)] and is therefore crucial for the superconductivity of K_3C_{60}. The occupied bandwidth W is about 130 meV. Based on the band dispersion and the calculation, we estimate the full bandwidth to be less than 200 meV [27], much smaller than the effective Coulomb interaction U of about 1 eV [28]. The Fermi velocity v_F is estimated to be about $7.5 \pm 0.5 \times 10^6$ cm/s compared to 1.8×10^7 cm/s in the density-functional theory (DFT) calculation [34], suggesting an effective electron mass $m^* = (1 + \lambda_{ep} + \lambda_{ee})m_b = (2.4 \pm 0.2)m_b$, where λ_{ep} and λ_{ee} are dimensionless EPC and electron-electron interaction parameters, and m_b is the bare mass [35]. The area of the FS (Supplemental Material, Fig. S2 [29]) suggests an electron density of about 2.9 ± 0.1 e$^-$/unit cell [27], or $(3.3 \pm 0.1) \times 10^{14}$ e$^-$/cm^2 [$(4.1 \pm 0.1) \times 10^{21}$ e$^-$/cm^3]. Using the DOS of 7.2 eV^{-1} per spin at E_F [17,36], we obtain a small Fermi energy of about 0.3 eV supposing all the t_{1u} electrons are free, consistent with previous results [37,38].

With decreasing temperature, the band dispersion becomes sharper while k_F remains nearly unchanged [Figs. 3(a)–3(d)]. At 8.5 K, we observe a strong renormalization of the band dispersion near −18, −54, and −85 meV, as shown by the dips in the integrated energy distribution curve (EDC) in Fig. 3(e), which will be discussed later. The leading edge of the EDC at k_F shifts towards high binding energies with decreasing temperature [Fig. 3(f)], evidencing the formation of superconducting gap, which is better visualized by the symmetrized ARPES spectra at 8.5 K in Fig. 3(g). By contrast, no gap is observed in the symmetrized spectra at 50 K [Fig. 3(h)]. Figure 3(i) shows the temperature evolution of the symmetrized EDCs at k_F. At 8.5 K, we observe a clear superconducting peak and superconducting gap [14]. With increasing temperature, the superconducting peak and superconducting gap gradually disappear. Interestingly, the symmetrized spectrum shows a dip at 30 K, which is an indication of a pseudogap that persists up to 40 K [14]. Figure 3(j) shows the temperature evolution of the leading-edge gap together with the temperature evolution of the gap depth extracted from STS measurements (Supplemental Material, Fig. S4 [29]). The fit of the gap depth to the BCS-type temperature evolution function suggests a superconducting transition temperature of 20.6 K. The fit of the symmetrized EDC to the Dynes model [32] gives a gap of about 4.3 meV at 8.5 K [black line in Fig. 3(i)], corresponding to the zero-temperature gap of about 4.5 meV. The reduced gap $2\Delta/k_BT_C$ is about 5, beyond the mean-field expectation of 3.5 [39]. Figure 3(k) presents the superconducting gap distribution in the momentum space (Supplemental Material, Fig. S3 [29]). Along different momentum directions, the superconducting gap remains constant within the accuracy of our experiment, which suggests a nodeless s-wavelike pairing symmetry. Consistently, the STS spectra show a U-shape superconducting gap at 4.7 K [Fig. 1(d)] [14].

Prominently, the band dispersion in Fig. 3(d) is strongly renormalized by multiple phonon modes [blue arrows in Figs. 3(d) and 3(e)]. We analyze the band renormalization by fitting the momentum distribution curves (MDCs) to Lorentzians (Supplemental Material, Fig. S5 [29]).

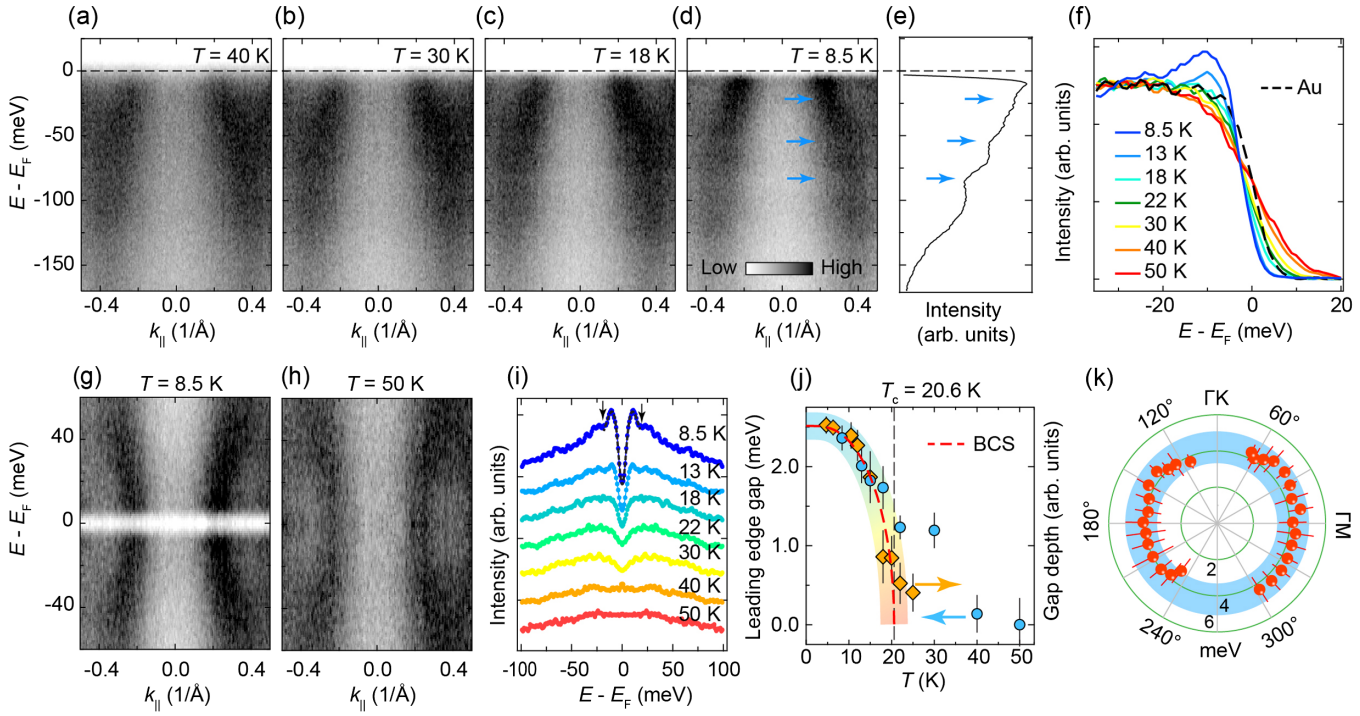

FIG. 3. (a)–(d) Band dispersion of 5 ML K_3C_{60} film along $\bar{\Gamma}\bar{M}$ near E_F collected at selected temperatures. (e) Integrated EDC at 8.5 K showing the reduction of spectral weight near binding energies of 18, 54, and 85 meV. (f) Comparison between the EDCs of K_3C_{60} at Fermi momentum (k_F) and polycrystalline gold showing the superconducting gap. (g),(h) Symmetrized ARPES spectra at 8.5 and 50 K, respectively. (i) Symmetrized EDCs integrated around k_F acquired at selected temperatures. The black dashed line is the fit to the Dynes function. The black arrows indicate the dip in the EDC. (j) Temperature dependent leading-edge gap from ARPES measurements (blue circles) and gap depth from STM measurements (orange diamonds). The red dashed line is the fit to the BCS model. (k) Angular distribution of superconducting gap extracted by fitting the symmetrized EDCs to the Dynes function.

The extracted band dispersions are shown in Fig. 4(a), from which we can observe the anomalies in the band dispersion near −54 and −85 meV, without noticeable change with temperature. Based on a linear bare band assumption, we extract the real and imaginary parts of the electron self-energy in Figs. 4(b) and 4(c). We observe peaklike features and the change of the slope in the real and imaginary parts of electron self-energy, respectively, which confirm the effect of EPC near −54 and −85 meV (thick gray lines).

The band renormalizations near −18 meV [manifested by the peak-dip-hump structure in Figs. 3(e) and 3(i)], −54 and −85 meV can be attributed to the intermolecular phonon mode, intramolecular $H_g(2)$ phonon, and intramolecular $H_g(3)$ phonon, respectively [17,40]. According to previous experiments and calculations, the $H_g(2)$ phonon mode indeed couples stronger with the electrons than the $H_g(3)$ phonon [17,40]. Therefore, it induces a more noticeable kink in the band dispersion [Fig. 3(d)]. The coupling to the other two modes, on the other hand, are manifested by the peak-dip-hump structure and the reduction of the spectral weight [Fig. 3(e)].

Interestingly, we observe a replica band at about 192 meV below the main band as shown in Figs. 4(d) and 4(e). Because of the strong EPC in K_3C_{60}, we attribute this band replication to the formation of polaron involving the $H_g(8)$ phonon mode that has been shown to strongly couple to the electrons among the H_g phonons in K_3C_{60} [17,41,42]. Since this phonon has an energy larger than the bandwidth near E_F, it induces a replica band instead of a kink in the dispersion, similar to the observation of the replica band in $FeSe/SrTiO_3$ [43].

The EPC parameter can be derived from the temperature dependence of the imaginary part of electron self-energy at high temperatures by $\mathrm{Im}\Sigma(E_F, T) = \lambda_{ep}\pi k_B T$ [44]. As shown in Fig. S6 in the Supplemental Material [29], λ_{ep} is estimated to be about 1.2 ± 0.3, about twice the value in previous results [15,17,41,45,46], suggesting a dominant role of EPC in the renormalization of effective electron mass. Moreover, from the slope change of the band dispersion [Fig. 4(a)], we get $\lambda_{ep} \sim 1.3$, which is consistent with the estimation by $\mathrm{Im}\Sigma(E_F, T)$.

In principle, the superconducting transition temperature can be estimated by McMillan-Allen-Dynes formula: $T_c = (\omega_{\ln}/1.2)\exp(-\{1.04(1+\lambda_{ep})/[\lambda_{ep} - \mu^*(1+0.62\lambda_{ep})]\})$ [47], where $\omega_{\ln}$ and μ^* are the logarithmic average phonon frequency and effective Coulomb pseudopotential, respectively. Using $\omega_{\ln} \approx 50 \pm 10$ meV and $\mu^* \approx 0.25$ [48–51], T_c is estimated to be 24 ± 5 K, consistent with the

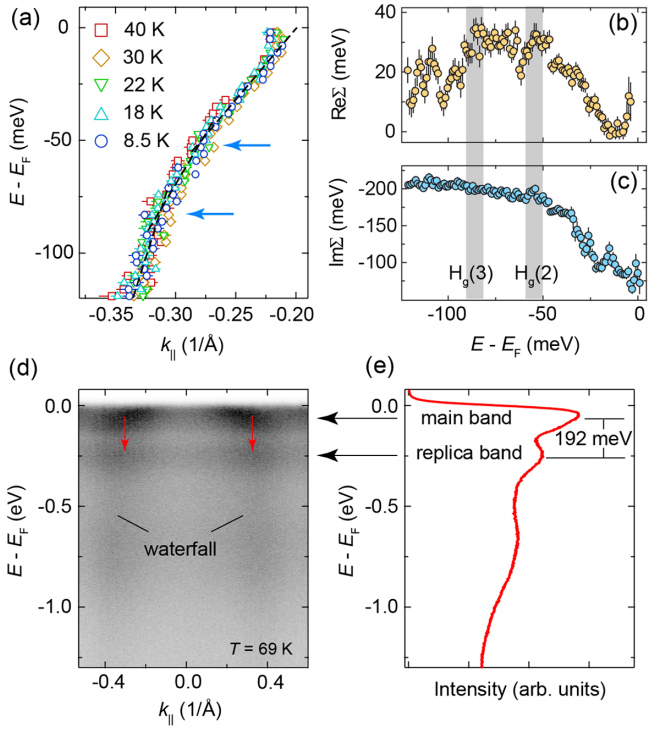

FIG. 4. (a) Comparison of the band dispersions at selected temperatures extracted from momentum distribution curve (MDC) fitting. The black dashed lines are the guides of eyes for the energy kinks in the band dispersion. (b),(c) Real and imaginary parts of the electron self-energy, respectively. (d) ARPES spectra in a large energy scale showing the band replication and waterfall-like band dispersion. (e) Integrated EDC obtained from (d).

experimental value. It is noteworthy, however, both $\omega_{\ln}$ and μ^* vary with a large uncertainty in the literature [17,40,52]. With the phonon energy of about 100 meV, μ^* up to 0.35 is required to reproduce the experimental T_c with McMillan equation [53]. Nonetheless, the revealed large EPC parameter, together with the large reduced superconducting gap $(2\Delta/k_BT_c) \approx 5$, suggests the strong-coupling nature of the superconductivity of K_3C_{60}.

On the other hand, we observe waterfall-like band dispersion in an energy window as large as 1.2 eV as shown in Fig. 4(d), reminiscent of the band dispersion of cuprate superconductors and other strongly correlated materials [54–56]. It suggests the impact of electronic correlation in the electronic structure, which is supported by the small W/U ratio [27,28], the small Fermi energy [57], and possibly large Coulomb pseudopotential of K_3C_{60}. Therefore, the electronic correlation should also be considered to fully understand alkali-fulleride superconductors.

In conclusion, we have comprehensively studied the band structure of alkali-doped C_{60} ultrathin films. In the superconducting K_3C_{60} films, we directly visualize the crucial band structure and band renormalization effects due to strong electron-phonon coupling. The analysis of ARPES spectra estimates the dimensionless electron-phonon coupling parameter to be about 1.2, evidencing the strong-coupling superconductivity of K_3C_{60}, supported by the large reduced superconducting gap. Further experiments such as isotope effects will deepen our understanding of the interplay between the band renormalizations and the novel superconductivity. Our results also reveal signatures of electron correlation, suggesting unusual interplay between the electron-phonon interaction and electronic correlation in the electronic structure and superconductivity of K_3C_{60} [13].

This work is funded by the National Key R&D program of China (Grants No. 2017YFA0304600, No. 2022YFA1403100, and No. 2022YFA1403200), the National Natural Science Foundation of China (Grants No. 12275148 and No. 11774190). L. X. Y. acknowledges the support from Tsingua University Initiative Scientific Research Program and the Fund of Science and Technology on Surface Physics and Chemistry Laboratory (No. XKFZ202102).

*yulin.chen@physics.ox.ac.uk
†lxyang@tsinghua.edu.cn

[1] A. F. Hebard, M. J. Rosseinsky, R. C. Haddon, D. W. Murphy, S. H. Glarum, T. T. M. Palstra, A. P. Ramirez, and A. R. Kortan, Superconductivity at 18 K in potassium-doped C_{60}, Nature (London) **350**, 600 (1991).

[2] M. J. Rosseinsky, A. P. Ramirez, S. H. Glarum, D. W. Murphy, R. C. Haddon, A. F. Hebard, T. T. M. Palstra, A. R. Kortan, S. M. Zahurak, and A. V. Makhija, Superconductivity at 28 K in Rb_xC_{60}, Phys. Rev. Lett. **66**, 2830 (1991).

[3] K. Tanigaki, T. W. Ebbesen, S. Saito, J. Mizuki, J. S. Tsai, Y. Kubo, and S. Kuroshima, Superconductivity at 33 K in $Cs_xRb_yC_{60}$, Nature (London) **352**, 222 (1991).

[4] A. Y. Ganin, Y. Takabayashi, Y. Z. Khimyak, S. Margadonna, A. Tamai, M. J. Rosseinsky, and K. Prassides, Bulk superconductivity at 38 K in a molecular system, Nat. Mater. **7**, 367 (2008).

[5] K. Holczer, O. Klein, S.-m. Huang, R. B. Kaner, K.-j. Fu, R. L. Whetten, and F. Diederich, Alkali-fulleride superconductors: Synthesis, composition, and diamagnetic shielding, Science **252**, 1154 (1991).

[6] R. M. Fleming, A. P. Ramirez, M. J. Rosseinsky, D. W. Murphy, R. C. Haddon, S. M. Zahurak, and A. V. Makhija, Relation of structure and superconducting transition temperatures in A_3C_{60}, Nature (London) **352**, 787 (1991).

[7] O. Zhou, Q. Zhu, J. E. Fischer, N. Coustel, G. B. M. Vaughan, P. A. Heiney, J. P. McCauley, and A. B. Smith, Compressibility of M_3C_{60} fullerene superconductors: Relation between T_c and lattice parameter, Science **255**, 833 (1992).

[8] Y. Takabayashi, A. Y. Ganin, P. Jeglič, D. Arčon, T. Takano, Y. Iwasa, Y. Ohishi, M. Takata, N. Takeshita, K. Prassides

et al., The disorder-free non-BCS superconductor Cs_3C_{60} emerges from an antiferromagnetic insulator parent state, Science **323**, 1585 (2009).

[9] A. Y. Ganin, Y. Takabayashi, P. Jeglič, D. Arčon, A. Potočnik, P. J. Baker, Y. Ohishi, M. T. McDonald, M. D. Tzirakis, A. McLennan *et al.*, Polymorphism control of superconductivity and magnetism in Cs_3C_{60} close to the Mott transition, Nature (London) **466**, 221 (2010).

[10] Y. Ihara, H. Alloul, P. Wzietek, D. Pontiroli, M. Mazzani, and M. Riccò, NMR Study of the Mott Transitions to Superconductivity in the Two Cs_3C_{60} Phases, Phys. Rev. Lett. **104**, 256402 (2010).

[11] Y. Takabayashi and K. Prassides, Unconventional high-T_c superconductivity in fullerides, Phil. Trans. R. Soc. A **374**, 20150320 (2016).

[12] M. Capone, M. Fabrizio, C. Castellani, and E. Tosatti, Colloquium: Modeling the unconventional superconducting properties of expanded A_3C_{60} fullerides, Rev. Mod. Phys. **81**, 943 (2009).

[13] Y. Nomura, S. Sakai, M. Capone, and R. Arita, Exotic *s*-wave superconductivity in alkali-doped fullerides, J. Phys. Condens. Matter **28**, 153001 (2016).

[14] M.-Q. Ren, S. Han, S.-Z. Wang, J.-Q. Fan, C.-L. Song, X.-C. Ma, and Q.-K. Xue, Direct Observation of Full-Gap Superconductivity and Pseudogap in Two-Dimensional Fullerides, Phys. Rev. Lett. **124**, 187001 (2020).

[15] M. Schluter, M. Lannoo, M. Needels, G. A. Baraff, and D. Tománek, Electron-Phonon Coupling and Superconductivity in Alkali-Intercalated C_{60} Solid, Phys. Rev. Lett. **68**, 526 (1992).

[16] A. A. Mostofi, J. R. Yates, G. Pizzi, Y.-S. Lee, I. Souza, D. Vanderbilt, and N. Marzari, An updated version of Wannier90: A tool for obtaining maximally-localised Wannier functions, Comput. Phys. Commun. **185**, 2309 (2014).

[17] O. Gunnarsson, Superconductivity in fullerides, Rev. Mod. Phys. **69**, 575 (1997).

[18] L. Degiorgi, G. Briceno, M. S. Fuhrer, A. Zettl, and P. Wachter, Optical measurements of the superconducting gap in single-crystal K_3C_{60} and Rb_3C_{60}, Nature (London) **369**, 541 (1994).

[19] R. H. Zadik, Y. Takabayashi, G. Klupp, R. H. Colman, A. Y. Ganin, A. Potočnik, P. Jeglič, D. Arčon, P. Matus, K. Kamarás *et al.*, Optimized unconventional superconductivity in a molecular Jahn-Teller metal, Sci. Adv. **1**, e1500059 (2015).

[20] C. Yue, S. Hoshino, A. Koga, and P. Werner, Unconventional pairing from local orbital fluctuations in strongly correlated A_3C_{60}, Phys. Rev. B **104**, 075107 (2021).

[21] M. Capone, M. Fabrizio, C. Castellani, and E. Tosatti, Strongly correlated superconductivity, Science **296**, 2364 (2002).

[22] S. C. Tiwari, A. Kashyap, A. K. Surana, R. K. Paliwal, and S. L. Kakani, Polaronic mechanism of superconductivity in doped fulleride systems, Int. J. Mod. Phys. B **23**, 615 (2009).

[23] T. Takahashi, S. Suzuki, T. Morikawa, H. Katayama-Yoshida, S. Hasegawa, H. Inokuchi, K. Seki, K. Kikuchi, S. Suzuki, K. Ikemoto *et al.*, Pseudo-Gap at the Fermi Level in K_3C_{60} Observed by Photoemission and Inverse Photoemission, Phys. Rev. Lett. **68**, 1232 (1992).

[24] J. E. Han, O. Gunnarsson, and V. H. Crespi, Strong Superconductivity with Local Jahn-Teller Phonons in C_{60} Solids, Phys. Rev. Lett. **90**, 167006 (2003).

[25] Y. Nomura, S. Sakai, M. Capone, and R. Arita, Unified understanding of superconductivity and Mott transition in alkali-doped fullerides from first principles, Sci. Adv. **1**, e1500568 (2015).

[26] H.-C. Jiang and S. Kivelson, Electronic pair binding and Hund's rule violations in doped C_{60}, Phys. Rev. B **93**, 165406 (2016).

[27] W. L. Yang, V. Brouet, X. J. Zhou, H. J. Choi, S. G. Louie, M. L. Cohen, S. A. Kellar, P. V. Bogdanov, A. Lanzara, A. Goldoni *et al.*, Band structure and Fermi surface of electron-doped C_{60} monolayers, Science **300**, 303 (2003).

[28] Y. Wang, R. Yamachika, A. Wachowiak, M. Grobis, and M. F. Crommie, Tuning fulleride electronic structure and molecular ordering via variable layer index, Nat. Mater. **7**, 194 (2008).

[29] See Supplemental Material at http://link.aps.org/supplemental/10.1103/PhysRevLett.130.216004 for details of (i) evolution of the band structure of C_{60} films, (ii) constant energy contours of C_{60} and K_3C_{60} films, (iii) extraction of the superconducting gap, (iv) temperature-dependent scanning tunneling spectroscopy measurements, (v) details about the fitting of the band dispersion, (vi) extraction of electron-phonon coupling constant, and (vii) phase separation at slight K doping, which includes Refs. [14,30–32].

[30] N. Haag, D. Lüftner, F. Haag, J. Seidel, L. L. Kelly, G. Zamborlini, M. Jugovac, V. Feyer, M. Aeschlimann, P. Puschnig *et al.*, Signatures of an atomic crystal in the band structure of a C_{60} thin film, Phys. Rev. B **101**, 165422 (2020).

[31] D. W. Latzke, C. Ojeda-Aristizabal, J. D. Denlinger, R. Reno, A. Zettl, and A. Lanzara, Orbital character effects in the photon energy and polarization dependence of pure C_{60} photoemission, ACS Nano **13**, 12710 (2019).

[32] R. C. Dynes, V. Narayanamurti, and J. P. Garno, Direct Measurement of Quasiparticle-Lifetime Broadening in a Strong-Coupled Superconductor, Phys. Rev. Lett. **41**, 1509 (1978).

[33] K. Sugawara, T. Sato, K. Kanetani, and T. Takahashi, Semiconductor–metal transition and band-gap tuning in quasi-free-standing epitaxial bilayer graphene on SiC, J. Phys. Soc. Jpn. **80**, 024705 (2011).

[34] S. C. Erwin and W. E. Pickett, Theoretical Fermi-surface properties and superconducting parameters for K_3C_{60}, Science **254**, 842 (1991).

[35] J. Jiang, K. Shimada, H. Hayashi, H. Iwasawa, Y. Aiura, H. Namatame, and M. Taniguchi, Coupling parameters of many-body interactions for the Al(100) surface state: A high-resolution angle-resolved photoemission spectroscopy study, Phys. Rev. B **84**, 155124 (2011).

[36] V. P. Antropov, I. I. Mazin, O. K. Andersen, A. I. Liechtenstein, and O. Jepsen, Dominance of the spin-dipolar NMR relaxation mechanism in fullerene superconductors, Phys. Rev. B **47**, 12373 (1993).

[37] D. Varshney, N. Kaurav, and K. K. Choudhary, Electrical transport in the normal state of K_3C_{60} fullerides: Polaron conduction, Supercond. Sci. Technol. **18**, 1259 (2005).

[38] D. Varshney, R. Jain, and N. Singn, Phonon drag and carrier diffusion contributions in thermoelectric power of K_3C_{60} fullerides, Int. J. Comput. Mater. Sci. Eng. **01**, 1250027 (2012).
[39] Z. Zhang, C.-C. Chen, and C. M. Lieber, Tunneling spectroscopy of M_3C_{60} superconductors: The energy gap, strong coupling, and superconductivity, Science **254**, 1619 (1991).
[40] P. Zhou, K.-A. Wang, P. C. Eklund, G. Dresselhaus, and M. S. Dresselhaus, Raman-scattering study of the electron-phonon interaction in M_3C_{60} ($M = K$,Rb), Phys. Rev. B **48**, 8412 (1993).
[41] J. Winter and H. Kuzmany, Landau damping and lifting of vibrational degeneracy in metallic potassium fulleride, Phys. Rev. B **53**, 655 (1996).
[42] O. Gunnarsson, H. Handschuh, P. S. Bechthold, B. Kessler, G. Ganteför, and W. Eberhardt, Photoemission Spectra of C_{60}^-: Electron-Phonon Coupling, Jahn-Teller Effect, and Superconductivity in the Fullerides, Phys. Rev. Lett. **74**, 1875 (1995).
[43] J. J. Lee, F. T. Schmitt, R. G. Moore, S. Johnston, Y. T. Cui, W. Li, M. Yi, Z. K. Liu, M. Hashimoto, Y. Zhang *et al.*, Interfacial mode coupling as the origin of the enhancement of T_c in FeSe films on $SrTiO_3$, Nature (London) **515**, 245 (2014).
[44] Z. H. Pan, A. V. Fedorov, D. Gardner, Y. S. Lee, S. Chu, and T. Valla, Measurement of an Exceptionally Weak Electron-Phonon Coupling on the Surface of the Topological Insulator Bi_2Se_3 Using Angle-Resolved Photoemission Spectroscopy, Phys. Rev. Lett. **108**, 187001 (2012).
[45] M. Mitrano, A. Cantaluppi, D. Nicoletti, S. Kaiser, A. Perucchi, S. Lupi, P. Di Pietro, D. Pontiroli, M. Riccò, S. R. Clark *et al.*, Possible light-induced superconductivity in K_3C_{60} at high temperature, Nature (London) **530**, 461 (2016).
[46] C. M. Varma, J. Zaanen, and K. Raghavachari, Superconductivity in the fullerenes, Science **254**, 989 (1991).
[47] P. B. Allen and R. C. Dynes, Transition temperature of strong-coupled superconductors reanalyzed, Phys. Rev. B **12**, 905 (1975).
[48] S. Satpathy, V. P. Antropov, O. K. Andersen, O. Jepsen, O. Gunnarsson, and A. I. Liechtenstein, Conduction-band structure of alkali-metal-doped C_{60}, Phys. Rev. B **46**, 1773 (1992).
[49] R.-S. Wang, D. Peng, J.-W. Hu, L.-N. Zong, and X.-J. Chen, Orientational ordering and electron-phonon interaction in K_3C_{60} superconductor, Carbon **195**, 1 (2022).
[50] D. Varshney, M. Varshney, R. K. Singh, and R. Mishra, Superconductivity in alkali metal doped fullerenes (K_3C_{60}): A phonon mechanism, J. Phys. Chem. Solids **60**, 579 (1999).
[51] V. Z. Kresin, Coupling strength in superconducting fullerenes, Phys. Rev. B **46**, 14883 (1992).
[52] I. I. Mazin, S. N. Rashkeev, V. P. Antropov, O. Jepsen, A. I. Liechtenstein, and O. K. Andersen, Quantitative theory of superconductivity in doped C_{60}, Phys. Rev. B **45**, 5114 (1992).
[53] O. Gunnarsson and G. Zwicknagl, Coulomb Pseudopotential, Screening and Superconductivity in C_{60}, Phys. Rev. Lett. **69**, 957 (1992).
[54] F. Ronning, K. M. Shen, N. P. Armitage, A. Damascelli, D. H. Lu, Z. X. Shen, L. L. Miller, and C. Kim, Anomalous high-energy dispersion in angle-resolved photoemission spectra from the insulating cuprate $Ca_2CuO_2Cl_2$, Phys. Rev. B **71**, 094518 (2005).
[55] Y. Liu, L. Yu, X. Jia, J. Zhao, H. Weng, Y. Peng, C. Chen, Z. Xie, D. Mou, J. He *et al.*, Anomalous high-energy waterfall-like electronic structure in 5d transition metal oxide Sr_2IrO_4 with a strong spin-orbit coupling, Sci. Rep. **5**, 13036 (2015).
[56] X. Gu, C. Chen, W. S. Wei, L. L. Gao, J. Y. Liu, X. Du, D. Pei, J. S. Zhou, R. Z. Xu, Z. X. Yin *et al.*, Robust kagome electronic structure in the topological quantum magnets XMn_6Sn_6 ($X = Dy$,Tb,Gd,Y), Phys. Rev. B **105**, 155108 (2022).
[57] E. Abrahams, Electron-electron scattering in alkali metals, Phys. Rev. **95**, 839 (1954).